一般セッション(口頭講演) | 4 JSAP-Optica Joint Symposia 2025：4.6 Terahertz Photonics

2025年9月10日(水) 13:30 ~ 16:30 | N203 (共通講義棟北)

[10p-N203-1~10] 4.6 Terahertz Photonics

大野 誠吾(東北大)、 村手 宏輔(名大)

英語発表

13:30 ~ 14:00

[10p-N203-1] [JSAP-Optica Joint Symposia Invited Talk] Development of a High-Power Laser-Integrated Backward Terahertz-wave Parametric Oscillator

○Yuma Takida[1], Hiroaki Minamide[1] (1.RIKEN RAP)

奨励賞エントリー 英語発表

14:00 ~ 14:15

[10p-N203-2] Terahertz-Wave Detection by Omnidirectional Phonon-Polariton Coupling and Amplification

○(D)Yuto Yoneda[1,2], Yuma Takida[2], Joselito E. Muldera[2], Alexander De Los Reyes[2], Yuehong Xu[2], Kunio Ishida[3], Hiroaki Minamide[1,2] (1.Chiba Univ., 2.RIKEN, 3.Utsunomiya Univ.)

奨励賞エントリー 英語発表

14:15 ~ 14:30

[10p-N203-3] Terahertz Time-Domain Ellipsometry of Liquids Without a Liquid Cell

○Atsuki Kamio[1], Verdad C. Agulto[1], Zixi Zhou[1], Kosaku Kato[1], Thanh Nhat Khoa Phan[1], Toshiyuki Iwamoto[1,2], Makoto Nakajima[1] (1.ILE, Univ. of Osaka, 2.Nippo Precision Co., Ltd)

奨励賞エントリー 英語発表

14:30 ~ 14:45

[10p-N203-4] Magneto-Optical Terahertz Time-Domain Ellipsometry of the Narrow-Gap Semiconductor InSb with Varying Carrier Densities

○(D)Zixi Zhao[1], Verdad C. Agulto[1], Atsuki Kamio[1], Kosaku Kato[1], Thanh Nhat Khoa Phan[1], Toshiyuki Iwamoto[1,2], Toshihiko Shimizu[1], Nobuhiko Sarukura[1], Makoto Nakajima[1] (1.ILE, Univ. of Osaka, 2.PNP)

英語発表

14:45 ~ 15:00

[10p-N203-5] Efficient THz Absorber based on Polymer-Hexaferrite Composite Films

○Justin LLANDRO[1,2], Zhehong LIU[2,3], Yoshito MURATA[4], Yoshihiro OKAMURA[3,4], Yasujiro TAGUCHI[2,3], Youtarou TAKAHASHI[3,4], Yoshinori TOKURA[3,4,5], Satoshi OKAMOTO[1,2] (1.Sumitomo Chemical, 2.RIKEN BZP, 3.RIKEN CEMS, 4.Univ. Tokyo, 5.Tokyo College)

奨励賞エントリー 英語発表

15:15 ~ 15:30

[10p-N203-6] Three-Dimensional Evaluation of the Cochlea Using Terahertz Near-Field Imaging

○(D)LUWEI ZHENG[1], Takeshi Fujita[2], Akinobu Kakigi[2], Hironaru Murakami[3], Masayoshi Tonouchi[4], Niu Zhengya[5], Kazunori Serita[5] (1.The Univ. of Osaka, 2.Kobe Univ., 3.Fukui Univ. of Tech., 4.Okayama Univ., 5.Waseda Univ.)

英語発表

15:30 ~ 15:45

[10p-N203-7] Investigation of the Physical Properties of Colloidal Indium Tin Oxide Nanocrystals Using Terahertz Spectroscopy

○(P)Daichi Eguchi[1], Kosaku Kato[1], Verdad C. Agulto[1], Makoto Nakajima[1] (1.The Univ. of Osaka)

英語発表
15:45 ~ 16:00
[10p-N203-8] Anisotropic Temperature Dependence of Carrier Transport in Beta-Gallium Oxide Epilayer Evaluated by Terahertz Time-Domain Spectroscopy

〇Shuang Liu[1], Verdad C. Agulto[1], Kosaku Kato[1], Toshiyuki Iwamoto[1,2], Thanh Nhat Khoa Phan[1], Hisashi Murakami[3], Yoshinao Kumagai[3], Makoto Nakajima[1] (1.UOsaka ILE, 2.Nippo Prec., 3.TAT Appli. Chem.)

英語発表
16:00 ~ 16:15
[10p-N203-9] Measurement of the Complex Anisotropy Ratio of the Nonlinear Optical Susceptibility in the Third Harmonic Generation by Terahertz Free-Electron Laser

〇(P)KHOA PHAN[1], You Wei Wang[1], Kosaku Kato[1], Verdad C. Agulto[1], Goro Isoyama[2], Makoto Nakajima[1] (1.UOsaka, ILE, 2.UOsaka, SANKEN)

英語発表
16:15 ~ 16:30
[10p-N203-10] Label-Free Detection of Glucose and Lactate Using Terahertz Chemical Microscope with Aptamer-Functionalized Sensing Plates

〇Yuta Mitsuda[1], Ryotaro Kubo[1], Hikaru Nakagawa[1], Toshihiko Kiwa[1], Jin Wang[1] (1.Graduate school of Okayama Univ.)

Development of a High-Power Laser-Integrated Backward Terahertz-wave Parametric Oscillator

Yuma Takida, Hiroaki Minamide

RIKEN Center for Advanced Photonics, RIKEN
E-mail: yuma.takida@riken.jp

1. Introduction

Non-destructive sensing using sub-terahertz (sub-THz) waves offers promising applications for industrial fields, thanks to their attractive properties, such as higher spatial resolution than millimeter waves. To realize a practical sensing system, a compact, robust, and high-output-power sub-THz-wave source is essential. As a strong candidate to meet these requirements, we recently demonstrated laser-driven backward THz-wave parametric oscillators (BW-TPOs) by using a slant-stripe-type periodically poled lithium niobate (PPLN) crystal [1–4]. The primary advantage of the BW-TPO is the mirrorless configuration owing to the counter-propagating interaction, where a pump photon is down-converted to backward-propagating THz-wave and forward-propagating idler photons without an optical cavity. This makes turn-key and alignment-free robust operation possible.

In this work, we have developed a compact all-in-one module of an injection seeded BW-TPO with a footprint size of 13.9 cm by 5.5 cm, as shown in Fig. 1.

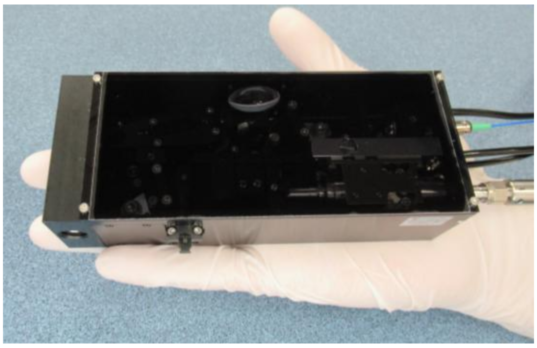

Fig. 1. Photograph of the developed palm-sized all-in-one BW-TPO module.

2. Experiment

In this BW-TPO module, the driving pump source of a passively Q-switched Nd:YAG microchip laser, BW-TPO gain medium of a slant-stripe-type PPLN crystal mounted on a motorized rotation stage, and all the optical components including a simple layout for injection seeding to the idler wavelength were assembled in a palm-sized package. From this compact module, the monochromatic backward-propagating THz-wave output was obtained with a maximum peak power of 15 W at 0.33 THz. Furthermore, by tuning the quasi-collinear phase-matching condition in the PPLN crystal, mode-hope-free frequency tunability from 0.29 to 0.35 THz was demonstrated.

Using the developed BW-TPO module, THz-wave imaging in reflection geometry was performed. The BW-TPO module and whole optical setup for reflection imaging were assembled on the optical breadboard that was mounted on a 2-axis motorized translation stage, while the position of the sample to be imaged was fixed. Fig. 2 shows the result of 0.3-THz reflection imaging with an area size of 150 mm by 200 mm with a 1-mm step without signal averaging. This result demonstrates the robust operation of the developed BW-TPO module.

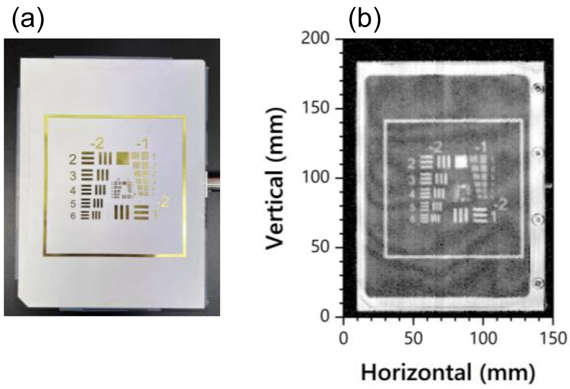

Fig. 2. (a) USAF 1951 test target pattern sample and (b) 0.3-THz reflection imaging result.

3. Conclusions

We have developed a palm-sized compact all-in-one BW-TPO module. Such a bright, frequency-tunable, and compact sub-THz-wave source is promising for real-world non-destructive sensing applications.

Acknowledgements

We thank Prof. H. Ito, Prof. M. Kumano, Dr. J. E. Muldera, Dr. D. Yadav, Dr. A. E. De Los Reyes, Dr. Y. Xu, Mr. Y. Yoneda, and Dr. K. Nawata for fruitful discussions. This work was supported in part by Innovative Science and Technology Initiative for Security, Grant Number JPJ004596, ATLA, Japan.

References

[1] K. Nawata *et al.*, Sci. Rep. **9** (2019) 726.
[2] Y. Takida *et al.*, APL Photon. **5** (2020) 061301.
[3] J. Muldera *et al.*, Opt. Express **31** (2023) 23966.
[4] J. Muldera *et al.*, Opt. Express **33** (2025) 22049.

Terahertz-Wave Detection by Omnidirectional Phonon-Polariton Coupling and Amplification

Chiba Univ. [1], RIKEN [2], Utsunomiya Univ.[3] ○Yuto Yoneda[1,2], Yuma Takida[2], Joselito E. Muldera[2], Alexander De Los Reyes[2], Yuehong Xu[2], Kunio Ishida[3] and Hiroaki Minamide[1,2]

E-mail: yuto.yoneda@riken.jp

Introduction

Frequency up-conversion detection, a theory proposed by M. Takatsuji in 1966 [1], enables ultra-low-noise detection of terahertz (THz) waves at room temperature. Backward terahertz-wave parametric oscillation (BW-TPO) has recently attracted attention for its potential to achieve low phase noise and high quantum conversion efficiency through narrowband oscillation [2]. However, nonlinear optical conversion requires strict phase matching, limiting the detection configuration—especially in BW-TPO, where THz-wave absorption restricts the interaction length.

In this study, we demonstrate a detection method utilizing phonon-polariton coupling and amplification by BW-TPO, which enables omnidirectional THz-wave detection without relying on conventional phase matching. Phonon-polaritons induced by THz waves generate dipole responses that provide omnidirectional gain in the plane orthogonal to the pump polarization, which are then up-converted and amplified in the phase-matched direction.

This approach lays the foundation for THz System on a Chip (T-SoC) platforms using meta surfaces, with potential applications in atmospheric monitoring, space debris detection, and remote sensing.

Experimental setup

Figure 1 shows the schematic of the experimental setup. BW-TPO was implemented using a slanted-stripe periodically poled lithium niobate (PPLN) crystal under quasi-collinear phase matching (QCPM). A pump pulse (0.46 ns, 100 Hz) was used, with 4.02 mJ on the generation side and 2.26 mJ on the detection side, below the oscillation threshold. A 500 mW CW seed laser was injected into the generation side. The generated THz wave was directed into the detection-side PPLN crystal along the direction counter to that of the phase-matching condition.

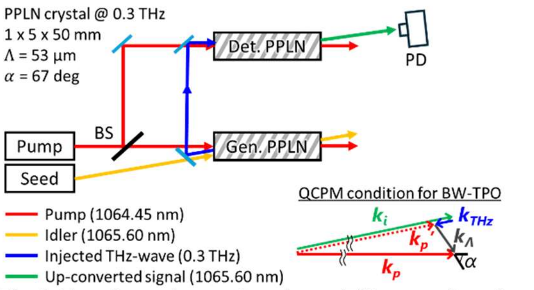

Fig. 1. Experimental setup for coherent THz-wave detection injected by counter direction of the phase-matching condition

Results and Discussion

Figure 2 shows the detection results of the up-converted signal. The red line indicates output with THz-wave injection, and the blue line shows the baseline without it. Similar setups were adapted for two other directions of THz-wave injection, lateral and phase-matched, respectively. In all cases, a high signal-to-noise ratio was observed, demonstrating robust detection regardless of incident direction.

The underlying detection mechanism proceeds in two distinct stages. First, incident THz-waves—regardless of their propagation direction—excite phonon modes that generate dipole oscillations near the threshold of parametric oscillation. These phonon-polariton interactions are inherently omnidirectional in the plane perpendicular to the pump polarization. Second, the dipole-induced modulation enables nonlinear up-conversion along the phase-matched direction, resulting in optical parametric amplification of the signal. This mechanism confirms that directional flexibility in THz-wave detection can be achieved through phonon-polariton coupling and amplification.

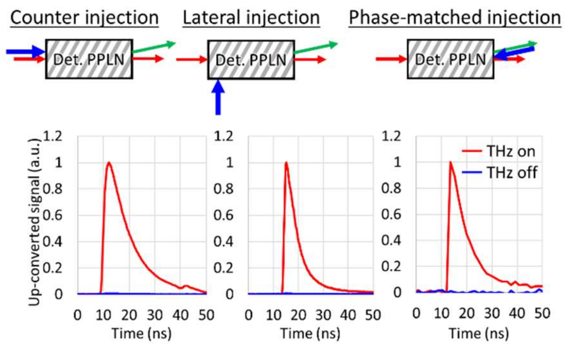

Fig. 2. Experimental result of up-converted signal for different injection direction

Acknowledgment

The authors would like to thank Prof. H. Ito of RIKEN/Tohoku University, Prof. M. Kumano of Tohoku University and Prof. M. Sato of Yamagata University for fruitful discussions. This work was supported by RIKEN Student Researcher Program and JST SPRING, Grant Number JPMJSP2109.

Reference

[1] M. Takatsuji, "Theory of Far Infrared Detection Using Nonlinear Optical Mixing," *Jpn. J. Appl. Phys.* **5**, 389 (1966)

[2] K. Nawata, Y. Tokizane, Y. Takida, and H. Minamide, "Tunable Backward Terahertz-wave Parametric Oscillation," *Sci. Rep.* **9**, 726 (2019).

Terahertz Time-Domain Ellipsometry of Liquids Without a Liquid Cell

Atsuki Kamio[1], Verdad C. Agulto[1], Zixi Zhao[1], Kosaku Kato[1], Thanh Nhat Khoa Phan[1], Toshiyuki Iwamoto,[1,2] and Makoto Nakajima[1]

[1] Institute of Laser Engineering, The University of Osaka, [2] Nippo Precision Co., Ltd.
E-mail: nakajima.makoto.ile@osaka-u.ac.jp

1. Introduction

Terahertz time-domain spectroscopy (THz-TDS) has become widely used as a non-contact technique capable of evaluating the dielectric and conductive properties of materials through the analysis of both amplitude and phase of the electric field. However, it remains challenging to measure liquid samples which strongly absorb terahertz radiation. In transmission THz-TDS, highly absorbing liquids require extremely thin liquid cell spacers to allow sufficient signal transmission. This requirement for thin sample layers can lead to measurement errors in the extracted optical constants, making high-precision evaluation difficult. In this study, terahertz time-domain ellipsometry (THz-TDE) was utilized to directly irradiate liquid samples with THz waves without using liquid cells.

2. Results

To demonstrate THz-TDE for liquid measurements, we investigated water which has known optical constants. Distilled water was placed in a 40 mm × 40 mm container and measured using THz-TDE without a window. THz-TDE was performed using Tera Evaluator, developed by Nippo Precision, Co., Ltd., with a spectral range from 1 THz to 3 THz [1-3]. The measurement chamber was purged with dry air to prevent THz absorption by water vapor. In the ellipsometry measurements, the reflected THz wave first passes through a rotating analyzer, which rotates from $\phi_A = 0°$ to 360° in 15° increments, before being recorded by the detector. The p- and s-polarized components were then extracted via nonlinear regression analysis based on the analyzer angle dependence of the detected signal. The detailed analysis method is discussed in [1]. This approach enables more accurate retrieval of the p and s polarization components compared to direct measurements of each component.

Fig. 1a shows the time-domain waveform magnified around the peak of the s-polarized terahertz wave reflected from the surface of water. As time progresses, the waveform exhibits a delay and a decrease in amplitude, which is attributed to a lowering of the water surface level caused by evaporation. These effects generate errors in the optical constants acquired from ellipsometry measurements. We developed a frequency-domain correction method to eliminate the effect of time-dependent changes in surface height. Specifically, the reflected waveform was Fourier-transformed, and the resulting amplitude and phase spectra were corrected to compensate for surface-level variation over time.

Fig. 1b presents the absorption spectra of water, calculated from the complex amplitude ratio (ellipsometric parameters) between p- and s-polarized components. It is evident that the absorption coefficient increases with frequency. In transmission THz-TDS, it is generally difficult to maintain a sufficient signal-to-noise ratio across a broad frequency range such as several terahertz due to the strong absorption by water. In contrast, with THz-TDE, both refractive index and absorption coefficient were successfully evaluated up to 3 THz. Moreover, the corrected measurement results were found to be consistent with previously reported data [4], confirming the validity of our correction approach.

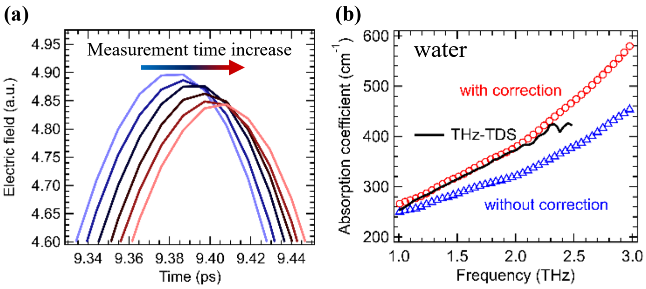

Fig. 1. **(a)** Time-domain waveforms of s-polarized THz pulses reflected from water surface, measured sequentially over time. The blue curve (leftmost) represents the earliest measurement, while the red curve (rightmost) corresponds to the latest. A gradual temporal delay and amplitude reduction are observed, indicating a decrease in the water surface level due to evaporation. **(b)** Absorption coefficient spectrum of water.

3. Conclusions

We demonstrated that our THz-TDE method, combined with the new analysis approach developed in this study for liquid samples, enables accurate characterization of volatile liquids without the use of a liquid cell. This result highlights the potential of THz-TDE as a robust technique for liquid analysis, especially for samples where conventional containment methods are impractical.

Acknowledgements

This work was supported by JSPS KAKENHI Grant Numbers JP24H00317, JP24H02232, and partially supported by JKA and its promotion funds from AUTORACE.

References

[1] V. C. Agulto et al., Sci. Rep. 11 (2021) 18129.
[2] V. C. Agulto et al., Opt. Lett., 50 (2025) 948-951.
[3] J. Wang et al., Nature, 631 (2024) 67-72.
[4] K. Jeong et al, J. Biomed. Opt., 18 (2013) 107008.

Magneto-Optical Terahertz Time-Domain Ellipsometry of the Narrow-Gap Semiconductor InSb with Varying Carrier Densities

Zixi Zhao[1], Verdad C. Agulto[1], Atsuki Kamio[1], Kosaku Kato[1], Thanh Nhat Khoa Phan[1], Toshiyuki Iwamoto[1,2], Toshihiko Shimizu[1], Nobuhiko Sarukura[1], and Makoto Nakajima[1]

[1] Institute of Laser Engineering, The University of Osaka, [2] Nippo Precision Co., Ltd.
E-mail: nakajima.makoto.ile@osaka-u.ac.jp

1. Introduction

Terahertz time-domain ellipsometry (THz-TDE) is an emerging terahertz (THz) technique that characterizes semiconductors by analyzing polarization changes of THz waves reflected from the sample. It combines the non-contact advantages of THz techniques with the high phase accuracy of ellipsometry, while also overcoming the limitations of terahertz time-domain spectroscopy (THz-TDS) related to sample thickness and carrier absorption. Additionally, THz-TDE can evaluate not only optical properties, but also carrier transport properties through Drude model fitting [1-4]. However, such analysis of carrier transport properties requires assumptions about parameters like effective mass, which is unfavorable for evaluating low-doped and narrow-gap semiconductors because effective mass depends on carrier density. To address this problem, the magneto-optical Kerr effect (MOKE) is incorporated into THz-TDE [5]. In a magnetic field, electrons undergo cyclotron motion, and the resonance frequency ω_c depends on the applied magnetic field and the electron effective mass. Therefore, electronic transport properties such as the effective mass can be effectively extracted without any assumptions.

2. Experiment

MO-THz-TDE measurements were performed using Tera Evaluator, developed by Nippo Precision, Co., Ltd., with a spectral range of 1-3 THz. An external magnetic field of 0.4 T perpendicular to the sample surface was applied by placing a permanent magnet beneath the sample. The THz wave was incident at an angle of 70°. By rotating the polarizer placed in front of the THz emitter, the incident polarization was modulated between p = s incidence and p-polarized incidence, allowing for the measurement of the complex reflection coefficient r_p without a magnetic field, as well as r_{sp} and r_{pp} under a magnetic field (where the first subscript represents the reflected polarization component and the second represents the incident polarization component).

In this study, undoped and n-type doped InSb (Indium Antimonide) wafers were evaluated. Both samples were cut along the [100] plane and single-side polished. The thicknesses of both samples are about 500 µm, and both samples are opaque to terahertz due to their high carrier absorption.

3. Results

The applied magnetic field induces asymmetric carrier motion via the Lorentz force, leading to the MOKE. As a result, the dielectric response of the sample is described by both the diagonal (ε_{xx}, ε_{zz}) and the off-diagonal (ε_{xy}) components of the dielectric tensor. The ε_{zz} represents the dielectric response along the direction parallel to the magnetic field. Thus, ε_{zz} for both samples remains consistent with their zero-field dielectric constants, as carriers are unaffected by the Lorentz force. The ε_{xx} and ε_{xy} of both samples, obtained from the complex reflection coefficients, are shown in Fig. 1. Doped InSb exhibits a stronger dielectric response in all directions. The real part of ε_{xx} for undoped InSb changes sign around 2.2 THz due to the low carrier density, which results in a low plasma frequency falling within the measurement range. In addition, ε_{xx} and ε_{xy} of the undoped InSb show oscillations near 2.8 THz, attributed to the magneto plasmon–phonon coupling effect. From the Drude model fitting, we obtained a plasma frequency of 5.5 THz, an effective mass of 0.020 m_0 (m_0=9.109×10^{-31} kg), and a carrier density of 1.13×10^{17} cm^{-3} for the doped InSb. For the undoped InSb, the plasma frequency was 2.2 THz, the effective mass was 0.018 m_0, and the carrier density was 1.67×10^{16} cm^{-3}.

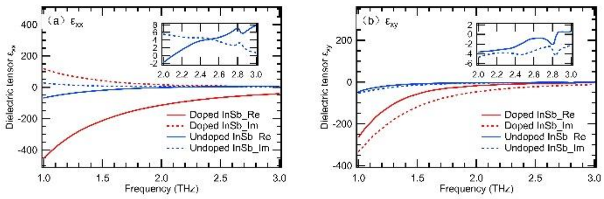

Fig. 1. Experimental spectra of (a) diagonal component ε_{xx} and (b) off-diagonal component ε_{xy} of dielectric tensor for doped and undoped InSb.

4. Conclusions

Doped and undoped InSb wafers were characterized using MO-THz-TDE. The dielectric tensors of both samples were successfully obtained and thus the electron effective mass is evaluated through the Drude model. These results demonstrate the ability of MO-THz-TDE to evaluate the optical and electron transport properties of narrow-gap semiconductors without any assumptions, making it a potential tool for investigating anisotropy of electron transport properties.

Acknowledgements

This work was supported by JSPS KAKENHI Grant Numbers JP24H00317, JP24H02232, JST SPRING Grant Number JPMJSP2138, and partially supported by JKA and its promotion funds from AUTORACE.

References

[1] V. C. Agulto, et al., Sci. Reports, **11** (2021) 18129.
[2] J. Wang, et al., Nature, **631** (2024) 67–72.
[3] Z. Zhao et al., Opt. Mater. X, **24** (2024) 100352.
[4] V. C. Agulto, et al., Opt. Lett. **50** (2025) 948-951.
[5] K. Yatsugi, et al., Appl. Phys. Lett. **98** (2011) 212108.

Efficient THz Absorber based on Polymer-Hexaferrite Composite Films

Sumitomo Chemical Co., Ltd.[1], RIKEN BZP[2], RIKEN CEMS[3], University of Tokyo[4], Tokyo College[5],

°Justin Llandro[1,2], Zhehong Liu[2,3], Yoshito Murata[4], Yoshihiro Okamura[3,4], Yasujiro Taguchi[2,3], Youtarou Takahashi[3,4], Yoshinori Tokura[3,4,5], Satoshi Okamoto[1,2]

E-mail: llandroj@sc.sumitomo-chem.co.jp

Terahertz radiation, particularly the frequency band 0.1~1 THz, is attracting strong interest as a contact-free probe of material properties in security scanning, quality inspection and non-invasive biosensing. However, the penetrating nature of THz radiation and its increasing use in communications also leads to high background noise in THz spectroscopy, making efficient THz absorbers vital. Existing approaches to large-area absorbers have focused on quasi-2D metasurfaces and 3D metamaterials based on nanotubes, microcoils, etc. where dimensions are tailored to THz resonances, and polymer composites which use highly conductive fillers to provide THz absorption. Such materials have been reported to exhibit high absorption but over a relatively narrow frequency range and/or above 1 THz [1].

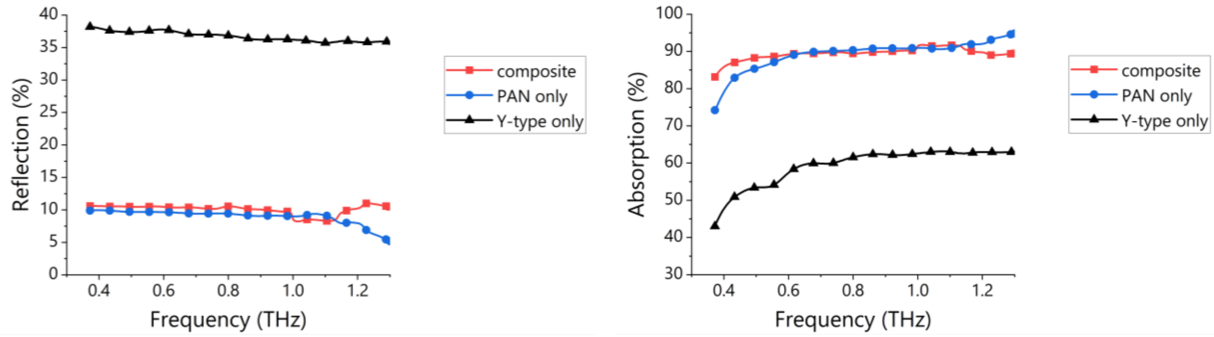

Figure 1: Reflection and absorption of polyacrylonitrile (PAN)/Y-type hexaferrite composite (1mm thick).

Here, we present an alternative approach to realizing a high-performance wide-band THz absorber, based on composites where both matrix and filler act as THz absorbers. Figure 1 shows initial results on a 1mm thick composite with a polar polymer matrix (polyacrylonitrile (PAN)) and a filler of micron-sized particles of multiferroic Y-type hexaferrite $Ba_{2-y}Sr_yCo_{2-x}Fe_{11+x}AlO_{22}$, which absorbs THz radiation by electro-magnon generation via its strong magneto-electric coupling [2]. Although PAN and single-crystal Y-type hexaferrite absorb most strongly at 0.7~0.8 THz, the frequency at which the composite reaches maximum absorption shifts down to 0.5 THz even with only 4% vol. of the hexaferrite. Work is ongoing to evaluate the effect of increased hexaferrite content and to compare the performance of PAN to other polymers [3].

[1] A.C. Ezika *et al.*, Polymer-Plastics Technology and Materials 64(11), 1633–1652 (2025).
[2] H. Shishikura *et al.*, Phys. Rev. Appl. **9**, 044033 (2018).
[3] T. Takahashi *et al.*, IEEE J. Trans. FM **127**(10), 593–598 (2007).

Three-Dimensional Evaluation of the Cochlea Using Terahertz Near-Field Imaging

Luwei Zheng[1], Takeshi Fujita[2], Akinobu Kakigi[2], Hironaru Murakami[1,3], Masayoshi Tonouchi[4], Niu Zhengya[5], and Kazunori Serita[5]

[1] Institute of Laser Engineering, The University of Osaka, [2] Department of Otolaryngology-Head and Neck Surgery, Graduate School of Medicine, Kobe University, [3] Department of Electrical, Electronic and Computer Engineering, Fukui University of Technology, [4] Research Institute for Interdisciplinary Science, Okayama University, [5] Graduate School of Information, Production, and Systems, Waseda University
E-mail: k_serita@aoni.waseda.jp

1. Introduction

Hearing impairment and loss are widespread conditions that impact a significant portion of the global population, greatly diminishing both communication abilities and overall quality of life [1]. These auditory issues are most commonly associated dysfunctions within the cochlea of the inner ear [2-4]. Achieving non-destructive imaging of the cochlea's internal structure with adequate spatial resolution remains a significant challenge. To address this, we successfully conducted the first non-destructive terahertz (THz) imaging of a mouse cochlea using a THz near-field point source microscope capable of micro-scale resolution [5,6]. High-accuracy three-dimensional (3D) THz time-of-flight (ToF) imaging and reconstruction were also demonstrated. This advancement lays the groundwork for future medical diagnostic applications, particularly in the early detection and evaluation of hearing-related disorders.

2. Method

The methodology employed in this study for 3D terahertz (THz) imaging and structural reconstruction of the cochlea involves three main stages: (1) two-dimensional (2D) data acquisition, (2) structural information extraction, and (3) 3D reconstruction. First, 2D time-domain THz images were obtained at various delay time points using a scanning point-source THz imaging system combined with the time-of-flight (ToF) technique. Second, an unsupervised machine learning algorithm—k-means clustering—was applied to classify the 2D THz images into distinct subgroups, enabling the separation of structural and non-structural regions. Finally, using the extracted structural data, a 3D point cloud was generated, and a 3D surface mesh was reconstructed through the Poisson surface reconstruction method. This approach demonstrates high reliability and flexibility, making it applicable to 3D reconstruction of a wide range of biological tissues.

3. Results

Fig. 1 shows the reconstructed 3D results, including 3D point cloud and surface mesh data. Fig. 1(a) and 1(b) show the 3D point cloud and surface mesh results, respectively. Fig. 1(c) shows a cross-sectional view of the 3D surface results shown in Fig. 1(b). The internal structure of the cochlea was easily and clearly observable, as indicated by the arrows in Figs. 1(b) and 1(c). Fig. 1(d) shows the bottom view of the reconstructed 3D surface mesh cochlea. The results demonstrate that the interior and exterior features of the cochlea can be successfully and clearly visualized.

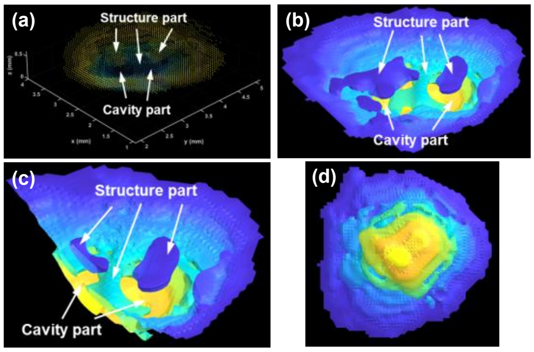

Figure 1 3D point cloud and surface mesh reconstruction.

4. Conclusions

In this study, we successfully visualized the internal structure of a mouse cochlea using terahertz (THz) near-field imaging with a micrometer-scale point source generated by laser irradiation (~20 μm spot size). The cochlea was placed on a GaAs substrate for effective imaging. 2D THz time-domain images were captured at various delay times, providing depth-resolved structural information. By applying the time-of-flight (ToF) principle, temporal data were converted into depth profiles. Structural features were extracted using *k*-means clustering, enabling 3D reconstruction through point cloud generation and Poisson surface meshing. This approach marks the first 3D THz imaging of cochlear structures and shows great potential for high-resolution imaging of biological tissues and early diagnosis of related diseases. Image analysis for achieving higher resolution and more detailed measurement results are presented.

Acknowledgements

This work is partially supported by the Japan Science and Technology Agency FOREST program (JPMJFR2029 and JPMJFR215F), the Japan Society for the Promotion of Science KAKENHI (JP23K22820, JP23H00184, and JP25K01294), and the China Scholarship Council (Grant No. 202206170007).

References

[1] S. G. Kujawa and M. C, Hear. Res. **330** (2015) 191–199.
[2] L. F. Corns *et al.*, Nat. Commun. **9** (2018) 4015
[3] Z. Wu *et al.*, Nat. Neurosci. *20* (2017) 24–33.
[4] P. Delmas *et al.*, Cell *155* (2013) 278-284.
[5] K. Serita *et al.*, Opt. Express 20 (2012) 12959-12965.
[6] L. Zheng *et al.*, Optica 12 (2025) 437-445.

Investigation of the Physical Properties of Colloidal Indium Tin Oxide Nanocrystals Using Terahertz Spectroscopy

Daichi Eguchi, Kosaku Kato, Verdad C. Agulto, Makoto Nakajima

ILE, The University of Osaka
E-mail: eguchi.daichi.ile@osaka-u.ac.jp

1. Introduction
Colloidal inorganic nanocrystals (NCs) consist of an inorganic core and organic ligands, which contribute to their physical properties and colloidal stability, respectively. Indium tin oxide (ITO) NCs exhibit a localized surface plasmon resonance (LSPR) band in the near-infrared (NIR) region, and the position of this band can be tuned by adjusting the ratio of indium to tin. Due to these properties, ITO NCs have attracted considerable attention for applications in photoenergy conversion materials [1]. The terahertz (THz) region is generally defined as the frequency range between approximately 0.1-10 THz. Although the terahertz region has lower photon energy compared to the visible range (1 THz = ~4.1 meV), it enables the measurement of physical phenomena—such as free electron behavior—that are not accessible with visible light. While the physical properties of bulk ITO have been investigated using terahertz spectroscopy [2], those of colloidal ITO NCs remain largely unexplored. In this study, we synthesized a series of ITO NCs with varying indium-to-tin ratios and different surface ligands, and investigated their physical properties using terahertz time-domain spectroscopy (THz-TDS).

2. Methods
The NCs were synthesized according to reported procedure [3]. Indium acetate and 2-ethylhexanoate tin were used as the indium and tin precursors, respectively. The indium-to-tin ratio was controlled by adjusting the molar ratio of the precursors. Ligand exchange from long alkyl chain ligands to inorganic ligands was carried out using BF_4^- (BF_4^-_ITO NCs) [4]. The obtained NCs were characterized by transmission electron microscopy, powder X-ray diffraction measurements, Fourier transform infrared spectroscopy, and steady-state absorption spectroscopy. The samples were prepared as pellets embedded in a matrix, and THz-TDS measurements were conducted in transmission mode using a femtosecond laser and a photoconductive antenna setup (TOPTICA, TeraFlash pro).

3. Results and discussion
The ITO NCs exhibited an LSPR band in the NIR region. After ligand exchange, the BF_4^--treated ITO NCs showed colloidal stability in polar solvents. This result indicates that the ligand exchange was successful, as the long alkyl chain ligands were non-polar and thus insoluble in polar solvents. Figure 1 presents the THz-TDS results. The amplitude of untreated ITO NCs was nearly identical to that of the matrix alone, while the BF_4^-_ITO NCs showed a reduced amplitude. This trend was not observed in control experiments using undoped In_2O_3 NCs. These results suggest that both tin doping and inorganic ligands contribute to changes in the terahertz time-domain waveform. From the time-domain data, the real and imaginary parts of the refractive index were calculated. In the BF_4^-_ITO NCs, the imaginary part increased at lower frequencies, whereas this trend was not observed in samples before ligand exchange or in undoped In_2O_3 NCs. These observations suggest that free electrons are delocalized due to the close interparticle distances.

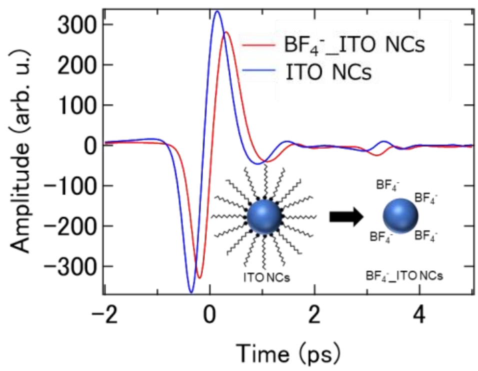

Figure 1. Time-domain waveforms for the BF_4^-_ITO NCs (red) and ITO NCs (Blue).

4. Conclusions
In summary, we synthesized ITO NCs with varying indium-to-tin ratios and ligands, and investigated their free electron behavior via terahertz spectroscopy. Our findings indicate that the presence of free carriers and the interparticle distance are important factors in terahertz spectroscopy of nanomaterials. This work may serve as a guideline for applying terahertz spectroscopy to other colloidal NC systems.

Acknowledgements
This work was supported by JSPS KAKENHI under Grant number 24H00317 and 25K17902 and The Hattori Hokokai Foundation.

References
[1] M. Sakamoto *et al.,* Nat. Commun. **10**, (2019) 406.
[2] T. Wang *et al*., Opt. Mater. Express **5**, (2015) 566-575.
[3] M. Kanehara *et al*., J. Am. Chem. Soc. (2009) **131**, 17736-17737.
[4] A. Dong *et al*., J. Am. Chem. Soc. (2011) **133**, 998-1006.

Anisotropic Temperature Dependence of Carrier Transport in Beta-Gallium Oxide Epilayer Evaluated by Terahertz Time-Domain Spectroscopy

Shuang Liu[1], Verdad C. Agulto[1], Toshiyuki Iwamoto[1,2], Kosaku Kato[1], Thanh Nhat Khoa Phan[1], Yoshinao Kumagai[3], Hisashi Murakami[3], and Makoto Nakajima[1]

[1]Institute of Laser Engineering, The University of Osaka
[2]Nippo Precision Co., Ltd.
[3]Department of Applied Chemistry, Tokyo University of Agriculture and Technology
E-mail: nakajima.makoto.ile@osaka-u.ac.jp

1. Introduction

Gallium oxide (Ga_2O_3), an emerging ultra-wide bandgap semiconductor (~4.9 eV), holds great promise for power electronics and deep-ultraviolet optoelectronic devices due to its high breakdown field and Baliga's figure of merit. Among its polymorphs, β-Ga_2O_3 is the most stable and exhibits strong anisotropy owing to its monoclinic structure. Terahertz time-domain spectroscopy (THz-TDS) offers a non-contact approach to probe anisotropic charge transport and phonon modes. While prior studies focused on room-temperature behavior [1-3], this work investigates anisotropic carrier transport in β-Ga_2O_3 over a wide temperature range, providing insights critical for device optimization.

In this study, we investigate the anisotropic terahertz response of β-Ga_2O_3 epitaxial layers along the a-axis [100] and b-axis [010] directions using THz-TDS. The measurements were conducted over a frequency range of 0.2-3 THz and a temperature range of 90-400 K. By fitting the experimental spectra with the Drude–Lorentz model, we quantitatively extracted key anisotropic transport parameters. These results offer fundamental insights into the direction-dependent carrier dynamics of β-Ga_2O_3 and provide valuable theoretical guidance for its integration into high-frequency electronic and optoelectronic devices.

2. Results

A 4.5 μm-thick Si-doped n-type β-Ga_2O_3 homoepitaxial layer was grown on a 647 μm-thick Fe-doped semi-insulating (001)-oriented β-Ga_2O_3 substrate. The highly doped epilayer have a carrier density of $\sim 5 \times 10^{17}$ cm^{-3} at room temperature measured by Hall method. THz-TDS measurements were conducted using a commercial system (Tera Prospector, Nippo Precision Co., Ltd.) equipped with photoconductive antennas for both THz pulse generation and detection. The sample was mounted in a liquid-nitrogen-cooled cryostat with precise temperature control from 90 to 400 K, housed in a dry-air-purged enclosure to minimize atmospheric water vapor absorption. The transmitted THz time-domain waveforms were recorded and subsequently Fourier-transformed to obtain the complex refractive index spectra.

The frequency-dependent complex refractive index of β-Ga_2O_3 was derived via Fourier transform and Fresnel transmission analysis. By fitting the spectra to Drude-Lorentz model considering only the effect of the first phonon mode of β-Ga_2O_3 on its terahertz response, we obtained the temperature-dependent parameters of carriers.

Figure 1 presents the temperature dependence of the DC conductivity, derived from the extracted plasma frequency and scattering time via the Drude-Lorentz model. At lower temperatures, the conductivity increases with the thermal activation of dopants, while at higher temperatures it decreases due to enhanced carrier scattering by lattice vibrations. The temperature dependence reveals clear anisotropy in carrier transport between the a- and b-axis directions. The observed anisotropic conductivity may come from slight differences in the electron effective mass, which become less pronounced at elevated temperatures. As temperature rises, DC conductivity anisotropy diminishes, consistent with electron mobility being increasingly limited by optical phonon scattering.

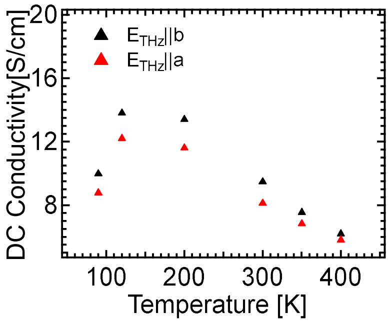

Fig. 1. The temperature dependence of DC conductivity along a- and b-axis.

3. Conclusions

We examined the anisotropic carrier transport in a Si-doped β-Ga_2O_3 epilayer along the [100] and [010] directions using THz-TDS over 90–400 K. The temperature-dependent anisotropy and its underlying mechanisms were discussed.

Acknowledgements

The authors are grateful to Dr. K. Goto for his support in sample fabrication. This work was supported by JSPS KAKENHI Grant Numbers JP24H00317, JP24H02232, and partially supported by JKA and its promotion funds from AUTORACE. This work was supported by JST SPRING, Grant Number JPMJSP2138.

References

[1] V. C. Agulto et al., *Appl. Phys. Lett.* **118** (2021) 042101.
[2] V. C. Agulto et al., *Sci Rep* **11**, 18129 (2021).
[3] J. Wang et al., *Nature* **631,** 67–72 (2024).

Measurement of the Complex Anisotropy Ratio of the Nonlinear Optical Susceptibility in the Third Harmonic Generation by Terahertz Free-Electron Laser

Thanh Nhat Khoa Phan[1], You Wei Wang[1], Kosaku Kato[1], Verdad C. Agulto[1], Goro Isoyama[2], Makoto Nakajima[1]

[1] Institute of Laser Engineering, The University of Osaka, [2] SANKEN, The University of Osaka,
E-mail: nakajima.makoto.ile@osaka-u.ac.jp

1. Introduction

The efficient nonlinear optical effect due to free carrier in the infrared region and terahertz (THz) region has been studied in narrow band gap semiconductor. The widely accepted mechanism has been attributed to the momentum-dependent effective mass of the free carrier [1]. This mechanism leads to a real value of the nonlinear susceptibility. Later, several authors extended the calculation and showed that the nonlinear susceptibility is a complex number [2,3], in which the momentum-dependent scattering time contributes to the imaginary part.

By utilizing an intense 4 THz beam from a THz free electron laser (FEL), we observed the angular anisotropy of the third harmonic generation (THG) from indium antimonide (InSb) [4], which revealed the contribution of the imaginary part of the nonlinear susceptibility originating from the momentum-scattering time relation.

2. Experiment

The FEL at the Research Laboratory for Quantum Beam Science at SANKEN, the University of Osaka [5], was used to excite the InSb samples. The FEL emits 5 macro-pulses per second, each containing around one hundred micro-pulses with picosecond duration. The output frequency of the laser was tuned to 4 THz. Radiation with frequency higher than 5 THz were filtered out by a low pass filter. Two wire-grid polarizers were used to set the laser beam polarization. The samples were rotated around their surface normal to change the angle ϕ (the azimuthal angle) between the crystal (010) axis and the polarization of the pumping beam. Then, a third wire-grid polarizer was inserted after the sample and rotated to selectively measured the intensity of the two orthogonal components $\boldsymbol{I}_{\parallel}$ and $\boldsymbol{I}_{\perp}$ of the THG beam, which correspond to the THG electric fields polarized parallel and perpendicular to that of the pumping beam. A DLaTGS (JASCO Corp.) detector was used to measure the signal intensity. A high pass filter was set before the detector to reject the residual 4-THz pumping beam.

3. Results

We observed THG signals with a peak frequency of 12 THz. Fig.1 shows the experiment result of the dependence of the two components $\boldsymbol{I}_{\parallel}$ (diamonds) and perpendicular $\boldsymbol{I}_{\perp}$ (circles) on the sample azimuthal angle. $\boldsymbol{I}_{\parallel}$ was modulated mainly with the angular cycle 90°, corresponding to the cos 4ϕ. However, the dips around 45° and 135° had a small local maximum around each center. This deviation from the cos 4ϕ-like shape is considered to reflect the cos 8ϕ term.

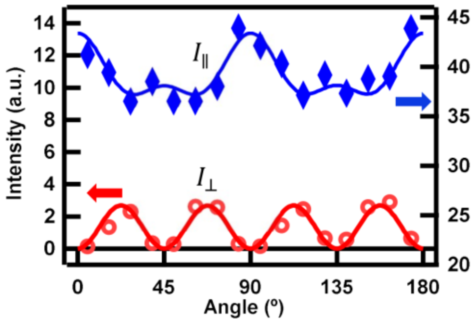

Fig.1. The dependence of THG intensity component $\boldsymbol{I}_{\parallel}$ and $\boldsymbol{I}_{\perp}$ on the sample azimuthal angle.

Meanwhile, $\boldsymbol{I}_{\perp}$ had an oscillation with the angular cycle 45° in agreement with the cos 8ϕ term. We evaluate the value of anisotropy ratio of the nonlinear susceptibility $\chi_R = \chi_2/\chi_1$ by fitting these results with theory equation [6]. The fitted curves were shown by the solid curves in Fig.1. From the fit, the absolute value and complex phase of χ_R were estimated to be $|\chi_R| = 0.38 \pm 0.02$ and $\theta_R = 58° \pm 4°$, respectively. The θ_R is far from zero and thus the imaginary part of the χ_R is considerably large. This result means that either or both of the nonlinear susceptibility tensor components χ_1 and χ_2 has a complex value.

4. Conclusion

The anisotropy ratios χ_R was extracted from the THz THG experimental data and was found to be complex values, the reason of which is proposed to be the non-negligible contribution of momentum dependence of the scattering time to the imaginary part of the nonlinear susceptibility.

Acknowledgements

This work was supported by Japan Society for the Promotion of Science (JSPS), grant numbers KAKENHI JP20H02206, JP23K17748, JP24H00317, JP24H02232.

References

[1] C. K. N. Patel *et al.*, Phys. Rev. Lett. **17** (1966) 1011.
[2] A. Mayer *et al.*, Phys. Rev. B **33** (1986) 6962.
[3] Charles C. Wang *et al.*, Phys. Rev. **188** (1969) 1291.
[4] Thanh Nhat Khoa Phan *et al.*, Opt. Lett. **49** (2024) 1073.
[5] Keigo Kawase *et al.,* Nucl. Instruments Methods Phys. Res. Sect. A **960** (2020) 163582.
[6] Thanh Nhat Khoa Phan *et al.*, Opt. Lett. **49**, (2024) 5039.

Label-Free Detection of Glucose and Lactate Using Terahertz Chemical Microscope with Aptamer-Functionalized Sensing Plates

Yuta Mitsuda[1], Ryotaro Kubo[1], Hikaru Nakagawa[1], Toshihiko Kiwa[1], Jin Wang[1]

[1] Graduate School of Interdisciplinary Science and Engineering in Health Systems, Okayama University

E-mail: p07k4tj7@s.okayama-u.ac.jp

1. Introduction

Glucose and lactate are key biomarkers for conditions such as diabetes and lactic acidosis, necessitating rapid and highly sensitive detection methods. Conventional approaches often rely on labels or enzymes, which involve complex procedures and limited sensitivity.

In this study, we employed a Terahertz Chemical Microscope (TCM) combined with aptamer-functionalized sensing plates to enable label-free and real-time detection of glucose and lactate. By utilizing dielectric changes at the sensing surface, this method offers a promising approach for advanced biosensing applications in the medical field.

2. Method

To detect glucose and lactate with high sensitivity, we employed a Terahertz Chemical Microscope (TCM) equipped with aptamer-functionalized Silicon-on-Sapphire (SOS) sensing plates. Each aptamer was immobilized onto the surface of the SiO_2 layer using a BS3-based crosslinking protocol following surface modification with NaOH and APTES [1].

After aptamer immobilization, target molecules (glucose or lactate) at various concentrations were introduced to the wells containing the sensing plates. Terahertz amplitude was measured before and after molecular binding. The spatial mapping of the THz amplitude was performed using an X-Y stage controlled via LabVIEW, and detection was carried out using photoconductive antenna sensors under femtosecond laser excitation.

3. Resalt

The terahertz amplitude changed significantly in response to the binding of glucose or lactate to their respective aptamers. This change correlated with concentration in both cases. As shown in Figures 1 and 2, the terahertz amplitude varied systematically with glucose and lactate concentrations, respectively.

For glucose, a monotonic increase in amplitude was observed with increasing concentration, demonstrating the feasibility of quantitative detection. For lactate, distinct amplitude shifts were confirmed across a wide dynamic range, from 0.1 mM to 100 mM.

The results confirmed that TCM enables highly sensitive, real-time, and label-free detection of small biomolecules. Reproducibility was verified through repeated measurements, and amplitude stability was maintained over the course of experiments.

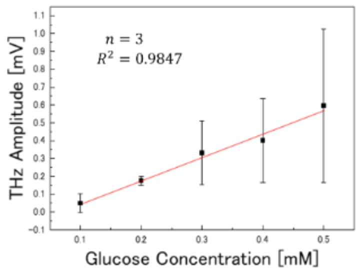

Fig.1 Correlation Between Glucose Concentration and Terahertz Amplitude

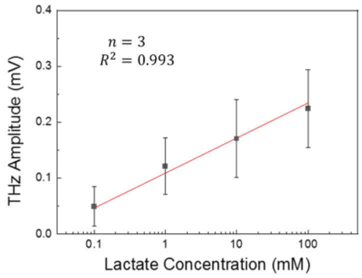

Fig.2 Correlation Between Lactate Concentration and Terahertz Amplitude

4. Conclusion

In this study, we investigated a detection method combining aptamer-functionalized sensors with terahertz chemical microscopy for identifying medically important small molecules such as glucose and lactate. The proposed approach is non-invasive and label-free, demonstrating its potential applicability to diabetes management and lactic acidosis monitoring.

References

[1]. Jin Wang, et al. Applied Physics Express, 16 (5), 052002, 2023.

[2]. T. Kiwa, A. Tenma, S. Takahashi, K. Sakai, and K. Tsukada, “Labe free immune assay using terahertz chemical microscope,” Sensors and Actuators B, 187, pp.8-11, 2013.

[3]. Kosei Morita, Yuta Mitsuda, Sota Yoshida, Toshihiko Kiwa, Jin Wang, “Mapping Surface Potential in DNA Aptamer–Neurochemical and Membrane–Ion Interactions on the SOS Substrate Using Terahertz Microscopy,” Biosensors, 15(1), pp.46 2025.